Abstract

RANGANATH, BHARGAV BINDIGANAVILE. Effects of Differential Diffusion on the Mutual Annihilation of Two Premixed Hydrogen-Air Flames. (Under the direction of Dr. Tarek Echekki)

The unsteady process of head on quenching of two laminar premixed hydrogen-air flames in one-dimension by mutual annihilation is investigated numerically using a detailed chemical mechanism and realistic transport. The process of annihilation through interactions is inevitable in highly corrugated turbulent flames, and contributes to turbulent flame shortening. Processes leading to mutual annihilation involve interactions that take place in the following stages: (1) interaction of preheat zones, which corresponds to the transport of heat and reactants, (2) interactions of the reaction layers as the flames merge, and finally (3) the process of burnout. The primary objective of this work is to study the effects of differential diffusion during the various events that occur during the unsteady process of annihilation. For the stoichiometric condition two cases are considered namely; a case where transport is based on prescribing non-unity Lewis numbers for all the species and a case with unity Lewis numbers prescribed for all the species. The latter case provides with a reference problem for the other flames considered. Because of the importance of differential diffusion during thermo-diffusive interactions, which are owed to the transport properties of H_2, relative to temperature and the oxidizer, two additional cases are considered. They correspond to lean and rich hydrogen-air flames. The results show that differential diffusion of H_2 plays an important role in determining the composition of the reacting mixture and thus, affects the final temperature and composition of the products. The differential diffusion of H_2 causes a deficiency of the fuel for the stoichiometric and lean cases thereby altering the rates of reactions involving H_2 while merger. For the rich case the deficiency caused by the differential diffusion is offset by the presence of excess H_2 in the reaction mixture. Due to these conditions for the rich flames and non-unity Lewis number case for the stoichiometric flame there is an increased production of the species O towards the end of merger.

Effects of Differential Diffusion on the Mutual Annihilation of Two Premixed Hydrogen-Air Flames

by

Bhargav Bindiganavile Ranganath

A thesis submitted to the Graduate Faculty of
North Carolina State University
in partial fulfillment of the
requirements for the Degree of
Master of Science

MECHANICAL AND AEROSPACE ENGINEERING

Raleigh

2003

APPROVED BY:

Chair of Advisory Committee

Biography

Bhargav Ranganath was born in Bangalore, India on 22nd June 1979. He is the son of the late B.V. Ranganath and B.R. Srimathi. He attended M.E.S. College and graduated pre-university in 1996.

Following pre-university Bhargav enrolled in the Mechanical Engineering program at M.S. Ramaiah institute of Technology affiliated to Bangalore University. In September 2000, he graduated with a bachelor of Engineer degree from Bangalore University.

Following graduation, Bhargav worked as a project assistant in The High Enthalpy Aerodynamics Laboratory at Indian Institute of Science, Bangalore for 10 months before enrolling in Graduate school at North Carolina State University. While pursuing a Master's of Science degree in Mechanical Engineering at N.C. State, he worked as a Research assistant with Dr. Tarek Echekki.

Acknowledgements

I would like to thank Dr. Echekki for his advising and believing in me while doing this work. Also, I would like to acknowledge the people from SANDIA for providing me with the code to carry out my work successfully. I would also like to thank all the faculty members at Bangalore University and NC state university with whom I have come in contact with while attending their lectures in shaping my approach towards solving a given problem. In particular I like to thank Dr. Hassan for letting me open the doors and think while attempting his open book exams. Last but not the least I would like to thank my mother and all my friends who put up with my emotions while completing my work.

Table of Contents

List of Figures

List of Tables

Chapter 1
Introduction

This chapter discusses the few of the earlier works relevant to the present problem, which concerns the process of mutual annihilation in premixed flames, the motivation behind the present work, the objective and finally presents an outline of the thesis.

1.1 Related work and motivation

There are two important classes of flames, namely premixed flames and non-premixed flames, which represent combustion processes in many practical applications. In non-premixed flames the fuel and oxidizer are initially not mixed. Diesel and gas-turbines are classic examples of non-premixed combustion. The fuel and oxidizer are mixed entirely by molecular diffusion process. The presence of turbulence enhances mixing in the large scales through coherent structures and at small scales through turbulent fluctuations. These flames are diffusion limited. In premixed flames, the fuel and oxidizer are mixed initially. The classic example is a gasoline driven engine or a Bunsen burner. A premixed flame propagates from the products into the reactants. In the presence of turbulence the overall burning of the fuel depends on the interfacial area between the reactants and the combustion products. The larger the area, i.e. higher the number of flamelets, the greater is the consumption of fuel and, hence, the higher is the heat release. But as the number of flamelets increases there is bound to be interaction among them, which lead to mutual annihilation and result in turbulent premixed flame shortening (Candel et. al 1990). These interactions involve the thermo-diffusive and reaction layer interactions and result in a change in the overall structure of the flames before they quench. Therefore, flames, in contrast to material surfaces in turbulence, may not cross paths without interactions, which involve a local quenching of the flame surface, the process of turbulent flame shortening. Another important consequence of mutual annihilation of interacting flamelets, in addition to its effect on the turbulent flame area, is its effect on the turbulent flame structure. Mutual annihilation may result in incomplete combustion, which may

leave extra unburnt hydrocarbons or result in a slow conversion of intermediates, and potentially an increased production in NO.

While it is difficult to investigate the unsteady process of mutual annihilation in detail experimentally, a number of simulations in recent years shed some important light on the process. Computations by Chen and Sohrab (1991) for a stoichiometric methane-air flame using a reduced chemistry showed an initial acceleration of the flame during the interactions of the reaction layers. They also found strong dependency of thermo-diffusive interactions on the Lewis number of the fuel and oxidizer i.e. relative diffusivities of the fuel and the oxidizer. Recent computations by Echekki et. al (1996) for stoichiometric methane-air flames involving detailed chemistry showed a twenty fold increase in the propagation velocity of the flame , which they found was due to a change in the balance between diffusion and reaction terms in the reaction zone during the interactions of the reaction layers. The works of Wichman and Vance (1997) showed the dependency of the process of annihilation on the Lewis number of the deficient species. For the Lewis number of the deficient species being less than unity they found that the process of annihilation was gradual and inexorable. However, for Lewis number greater than unity for the deficient species the process of annihilation was rapid. Recent works by Im and Chen (2002) have shown an increase in the consumption speed for the fuel and oxidizer due to an overshoot in the radical pool during the upstream interactions of rich twin hydrogen-air flame in 2-D turbulence.

1.2 Objective

Since the mutual annihilation of two interacting flames involves in principle the progressive interaction of the various layers from preheat to reaction layers, an understanding of the role of transport and chemistry is important. Differential diffusion effects have already been identified for methane-air flames during the unsteady interactions of the reaction layers, as the primary fuel is consumed, and the consumption layers of the secondary fuels, CO and H_2, merge yielding an important increase in the radical pool, and subsequent acceleration of the mutual annihilation process. Differential diffusion may play important roles during thermo-diffusive interactions for fuels that are

characterized by their disparate rates of diffusion with respect to heat or the oxidizer. This may be the case for hydrogen-air flames or propane-air flames. Different rates of diffusion may result in a shift in the stoichiometry of the flame during mutual annihilation, with consequences on the remaining reaction layer interactions.

The objective of the present work is to study the effect of differential diffusion of hydrogen on the mutual annihilation two premixed hydrogen-air flames in one dimension. The scope is to study differential diffusion of H_2 effects on the thermo-diffusive interactions and how they affect the final product and temperature after the merger of the reaction layers. A number of strategies are adopted to identify the role of differential diffusion in hydrogen-air flames. First, stoichiometric flame simulations are implemented for unity and non-unity Lewis numbers to discern the role of differential diffusion. The second strategy consists of running two different equivalence ratios, including lean and rich hydrogen-air mixtures.

1.3 Outline

The rest of the document is divided into three chapters.

- In chapter 2, the numerical implementations and the diagnostic tools are discussed. Under numerical implementation the governing equations, boundary conditions, mixture properties and the chemical mechanism used are discussed. Under the diagnostics section the various tools like equivalence ratio, evolution of the leading edges, consumption speeds for fuel and oxidizer, the consumption and production rates of the intermediates and evolution of the rates of reaction progress are discussed.
- In chapter 3 the results for the stoichiometric case with unity and non-unity Lewis numbers formulations are discussed first, followed by the results for rich and lean flames.
- Chapter 4 offers with the conclusions where the results are summarized for the three flames considered.

Chapter 2
Numerical Implementation and Diagnostics

In this chapter the solution scheme and the tools used for the numerical diagnostics are discussed. First the governing equations, boundary conditions, mixture properties, initial profiles and run conditions are discussed. These form the part of the solution scheme. Next the different tools used for the diagnostics of the process of flame interactions are discussed.

2.1 Governing Equations

The numerical scheme is based on the solution of the conservation equations for a compressible flow. The governing equations are

- Continuity equation

$$\frac{\partial \rho}{\partial t} + \frac{\partial (\rho u_j)}{\partial x_j} = 0 \qquad \textbf{Equation 2-1}$$

- Momentum equation

$$\frac{\partial (\rho u_i)}{\partial t} + \frac{\partial (\rho u_i u_j)}{\partial x_j} = -\frac{\partial p}{\partial x_i} + \frac{\partial \tau_{ij}}{\partial x_j} \qquad \textbf{Equation 2-2}$$

- Energy equation

$$\frac{\partial (\rho e_t)}{\partial t} + \frac{\partial (e_t + p) u_j}{\partial x_j} = \frac{\partial (u_j \tau_{ij})}{\partial x_i} - \frac{\partial q_j^{"}}{\partial x_j} \qquad \textbf{Equation 2-3}$$

- Species equation

$$\frac{\partial (\rho Y_k)}{\partial t} + \frac{\partial (\rho Y_k u_j)}{\partial x_j} = -\frac{\partial (\rho Y_k V_{D\,kj})}{\partial x_j} + W_k \dot{\omega}_k \qquad \textbf{Equation 2-4}$$

The pressure is computed from equation of state $p = \rho RT$. In the above equations ρ is the density of the reacting mixture, u_i is the velocity along the x_i direction, V_{Dkj} is the diffusion velocity of the k^{th} species along x_j direction, $q_j^{"}$ is the heat flux given

by $q''_j = -\lambda \frac{\partial T}{\partial x_j} + \rho \sum_{k=1}^{N} h_k Y_k V_{Dkj}$, λ is the thermal conductivity, T is the temperature, e_t is the total energy given by the sum of the internal energy and the kinetic energy $e_t = e + 1/2\left(u_i u_i\right)$ and internal energy $e = \sum_{k=1}^{n} Y_k h_k - \frac{p}{\rho}$, enthalpy $h_k = h_k^{\circ} + \int_{T^{\circ}}^{T} c_{p,k}(T) dT$ (superscript o refers to reference condition), τ_{ij} is the component of the stress tensor given by $\tau_{ij} = \mu\left(\frac{\partial u_i}{\partial x_j} + \frac{\partial u_j}{\partial x_i} - \frac{2}{3}\delta_{ij}\frac{\partial u_k}{\partial x_k}\right)$, δ_{ij} is the Kronecker delta, p is the pressure, R is the gas constant, Y_k is the mass fraction of the k^{th} species, $\dot{\omega}_k$ is the molar production rate of the k^{th} species and W_k is the molecular weight of the k^{th} species.

The production rate $\dot{\omega}_k$ for the k^{th} species is the result of the contribution of the elementary reactions involving the k^{th} species and is obtained as the summation of the rate of progress variables for all the elementary reactions involving the k^{th} species weighted by the difference in the stoichiometric coefficients for those reactions. It is assumed that all the reactions proceed according to the law of mass action.

$\dot{\omega}_k = \sum \nu_{ki} q_i$ Where ν_{ki} is the stoichiometric coefficient of the k^{th} species for the i^{th} reaction and q_i is the rate of progress variable.

$$q_i = k_{fi} \prod_{k=1}^{N} \left[X_k\right]^{\nu_{ki}'} - k_{ri} \prod_{k=1}^{N} \left[X_k\right]^{\nu_{ki}''} \qquad \textbf{Equation 2-5}$$

Where k_{fi} and k_{ri} are the forward and reverse rate coefficients for the i^{th} reaction in the modified Arrhenius form, X_k is the concentration of the k^{th} species and ν_{ki}' .and ν_{ki}'' are the forward and reverse stoichiometric coefficients for the i^{th} reaction involving the k^{th} species.

2.2 Solution Scheme

The above equations are solved using an explicit eighth order finite difference scheme in space (Kennedy et. al, 1994) and a fourth order accurate Range-Kutta scheme in time (Kennedy et. al, 2000).

2.2.1 Boundary Conditions

The boundary conditions are based on the NSCBC boundary conditions, which were originally formulated by Poinsot and Lele (1991) and adopted to the present governing equations by Mahalingam (1994), which account for variable transport and thermodynamic properties. The boundary condition is non-reflecting is *x*, meaning any characteristic waves with a net component leaving the domain are allowed to exit the domain, while no disturbances from outside the domain are allowed to enter it.

2.2.2 Properties of Reacting Mixture

The properties of the gas mixture change with temperature and composition over the domain. Hence temperature dependent properties are employed for the simulation.

The thermal conductivity is modeled through the approximation suggested by Smooke and Giovangigli (1991) as

$\lambda = \bar{c}_p \, A\left(\frac{T}{T_\circ}\right)^r$ Where $c_p(T) = \sum_{\alpha=1}^{\bar{N}} Y_\alpha c_{p\alpha}(T)$ is the specific heat of the reacting mixture, $c_{p\alpha}$ is the specific heat of the individual species obtained as polynomial functions of temperature using the CHEMKIN thermodynamic database (Kee et. al. 1987), T_o is the reference temperature, T is the actual temperature in the domain, A and r are the constants obtained from the fit given by $A = 2.58 \times 10^{-4}\ g/cm - s$ and $r = 0.7$.

In the present work, the mass transfer through temperature gradient (Soret effect) and energy transport through concentration gradients (Dufour effect) are neglected. The transport is based on the prescription of Lewis numbers formulation for individual species obtained from Smooke and Giovangigli (1991). From an initial solution obtained from PREMIX, the diffusion coefficients for the individual species are computed using the mixture averaged method. From these diffusion coefficients the Lewis numbers are

computed for a temperature range between 500 and 2500 K. The diffusion coefficients for DNS are then computed as

$D_{a,\alpha} = \dfrac{\lambda}{\rho Le_\alpha \bar{c}_p}$. The Lewis numbers for stoichiometric, rich and lean conditions are given in the Table 2.1, Table 2.2 and Table 2.3 respectively. The Prandtl number $P_r = \dfrac{\mu c_p}{\lambda}$ is set to a constant of *0.708*.

2.2.3 Chemical Mechanisms

Chemistry is based on the detailed hydrogen mechanism of Yetter et al (1991) with 9 species as listed in Table 2.1 and 19 reversible elementary reactions. The mechanism is presented in the Table 2.4.

2.2.4 Initial profiles for DNS

Sandia's PREMIX code is used to obtain the initial profiles for temperature, species mass fractions, density and pressure for the DNS simulations. A freely propagating adiabatic flame is considered. The location of the flame is fixed by specifying the temperature at that location. This point is selected such that the species and temperature gradients almost vanish at the cold boundary. The solution from PREMIX is based on a non-uniform grid form. The profiles of velocity, species and temperature are then mapped to a uniform grid and mirrored to obtain two symmetric flames, which later interact in the upstream direction in the DNS simulations.

2.3 Run Conditions

The computations are carried out using Sandia's S3D code. This code was developed for a three dimensional case, and in the present work it is implemented for solving the conservative equation is one dimension. The domain length is 10.5 cm long with 10,504 spatially-uniform grid points. Non-reflecting boundary conditions are applied along the *x* direction. Three cases are considered; stoichiometric mixture, rich mixture and lean mixture. The initial temperature is 300 K and the pressure is 1 Atm.

2.4 Diagnostics

Mutual annihilation of two flames in one dimension is an unsteady process. The solution obtained from PREMIX is made to attain steady state in DNS before any interaction occurs between them. For this purpose initially the flames are sufficiently spaced apart. DNS yields detailed information about the flow and scalar fields that depict the process of annihilation. Additional quantities are derived from these simulations to better understand the process of mutual annihilation. They are discussed in the following sections.

2.4.1 Equivalence Ratio

The equivalence ratio is a measure of the relative ratios of the fuel to the oxidizer. It is generally evaluated for reactants prior to their entry into the preheat and reaction zones. Since the concentrations of the fuel and oxidizer change over the domain it is convenient to obtain the equivalence ratio by tracking the elements. Thus, the equivalence ratio can be computed at any location in the domain. The mixture fraction is computed based on the definition by Bilger et. al. (1990) as

$$\xi = \frac{\left(Y_H - Y_{H,o}\right)/(2W_H) - \left(Y_O - Y_{O,o}\right)/W_O}{\left(Y_{H,f} - Y_{H,o}\right)/(2W_H) - \left(Y_{O,f} - Y_{O,o}\right)/W_O} \qquad \textbf{Equation 2-6}$$

Where W_i*'s* are the atomic weights, subscripts *f* and *o* refer to fuel and oxidizer side. The Y_i's are the elemental mass fractions computed as $Y_i = \sum_{j=1}^{N} \mu_{i,j} Y_j$, for *N* species.

A polynomial fit is obtained for various values of the mixture fractions and the corresponding equivalence ratios. This fit is used to obtain the equivalence ratio at all locations in the domain. Figure 2.1 shows the plot of the fit.

2.4.2 Consumption Speed

Consumption speed is defined as the integrated reaction rate of the fuel or oxidizer normalized to yield units of speed (m/s). The consumption speed corresponds exactly to the laminar 1D flame speed at steady state. The consumption speed is given as:

$$S_C = \frac{\int_{x=0}^{L} \dot{\omega}_\alpha \, dx}{\rho_u \left(Y_{\alpha,u} - Y_{\alpha,b} \right)} \qquad \textbf{Equation 2-7}$$

Where $\dot{\omega}_\alpha$ = reaction rate for species α, *Y*'s are the mass fractions and ρ_u is the unburnt gas density.

The consumption speed is a scalar quantity, which gives the rate at which the fuel or oxidizer is consumed at any time. The process of interaction is unsteady in nature and the consumption speed for the fuel and oxidizer change during these interactions due to a competition for the reactants.

2.4.3 Leading Edges

The choice of leading edge is arbitrary and in the present work it is defined as the location where normalized Temperature or the Species mass fractions vary by 5% of initial value at the symmetry line. Leading edge location gives the location of the species or temperature diffusive layers in the domain. The slope of the leading edge gives the displacement speed of the respective iso-contour i.e. the rate at which these layers diffuse within the domain. Tracking the leading edges gives us an idea as how fast the merger of the various layers takes place. The species mass fractions are normalized by their initial values and the temperature is normalized to obtain a complimentary progress variable such that before any interaction among the flames the normalized quantities are equal to one. The expression for the normalized temperature is defined as: $T_{normlized} = \frac{T_b - T}{T_b - T_u}$, where the subscripts *b* and *u* represent the burnt and unburnt conditions.

2.4.4 Contribution of diffusive, convective and reaction terms on the unsteady term

Consider the species equation;

$$\frac{\partial(\rho Y_k)}{\partial t} = -\frac{\partial(\rho Y_k u_j)}{\partial x_j} - \frac{\partial(\rho Y_k V_{D\,kj})}{\partial x_j} + W_k \dot{\omega}_k$$

The term on the left-hand side is the unsteady term. The first term on the right-hand side is the contribution due to convective term, the second term is the contribution due to diffusive term and the last term is the contribution due to reaction term. By tracking these terms we can find the direction in which the species diffuse and which terms balance the reaction term in the reaction zone.

The terms on the right-hand side of the species equation are evaluated over the entire domain and plotted as a function of distance. It gives qualitative information as to which term influences the unsteady term in a particular zone of the flame.

2.4.5 Evolution of Consumption and Production layers for Radicals

The reaction layers of the radicals are made of more than one consumption and production layers. The consumption and production layers are integrated and evaluated separately and plotted as a function of time. These integrated quantities indicate how the consumption and production layers evolve when the two flames interact.

Integrated production rate is given by $\int_{x1}^{x2} \dot{\omega}_{production}\, dx$ and integrated consumption rate is given by $\int_{x1}^{x2} \dot{\omega}_{consumption}\, dx$. These quantities are normalized by their initial values.

2.4.6 Integrated reaction rate of progress

Different elementary reactions contribute differently to the consumption of reactants and heat generation. By plotting the integrated reaction rate of progress for these elementary reactions one can obtain information as to the behavior of the reactions during the interactions. Reaction rate of progress for the elementary reactions are integrated over the entire domain and plotted as a function of time.

Integrated rate of reaction progress = $\int_{x=0}^{L} q_i dx$ where q_i is the rate of reaction progress. These quantities are normalized by their initial values.

2.4.7 Characteristic scales

Characteristic scales are defined for length and time for the purpose of normalizing the results.

For length: The flame thickness or the thermal thickness is defined for the length scale. It is defined as the ratio of the temperature difference across the flame to the maximum temperature gradient:

$$\delta_f = \frac{T_b - T_u}{(dT/dx)_{\max}}$$

For time: Flame time is defined as the ratio of the flame thickness to the unperturbed laminar flame speed:

$$t_f = \frac{\delta_f}{\overset{\circ}{S}_L}$$

These quantities are constants and are based on the initial conditions, which represent the steady state conditions.

Species	H_2	O_2	O	OH	H_2O	H	HO_2	H_2O_2	N_2
Le #	0.33	1.20	0.78	0.79	0.88	0.20	1.20	1.21	1.35

Table 2-1: Lewis numbers for the nine species–stoichiometric mixture.

Species	H_2	O_2	O	OH	H_2O	H	HO_2	H_2O_2	N_2
Le #	0.37	1.36	0.89	0.91	1.02	0.23	1.36	1.37	1.63

Table 2-2: Lewis numbers for the nine species–rich mixture.

Species	H_2	O_2	O	OH	H_2O	H	HO_2	H_2O_2	N_2
Le #	0.31	1.13	0.72	0.74	0.83	0.18	1.12	1.13	1.19

Table 2-3: Lewis numbers for the nine species–lean mixture.

	Reaction	**A**	***β***	**Ea**
1	$H + O_2 \Leftrightarrow O + OH$	1.92×10^{14}	0.0	16.44
2	$O + H_2 \Leftrightarrow H + OH$	5.02×10^{04}	2.67	6.29
3	$OH + H_2 \Leftrightarrow H_2O + H$	2.16×10^{08}	1.51	3.43
4	$OH + OH \Leftrightarrow H_2O + O$	1.23×10^{04}	2.62	-1.88
5	$H_2 + M \Leftrightarrow H + H + M$	4.57×10^{19}	-1.4	104.4
6	$O + O + M \Leftrightarrow O_2 + M$	6.17×10^{15}	-0.5	0.0
7	$O + H + M \Leftrightarrow OH + M$	4.72×10^{18}	-1.0	0.0
8	$H + OH + M \Leftrightarrow H_2O + M$	2.25×10^{22}	-2.0	0.0
9	$H + O_2 + M \Leftrightarrow HO_2 + M$	6.17×10^{19}	-1.42	0.0
10	$HO_2 + H \Leftrightarrow H_2 + O_2$	6.63×10^{13}	0.0	2.13
11	$HO_2 + H \Leftrightarrow OH + OH$	1.69×10^{14}	0.0	0.87
12	$HO_2 + O \Leftrightarrow OH + O_2$	1.81×10^{13}	0.0	-0.4
13	$HO_2 + OH \Leftrightarrow H_2O + O_2$	1.45×10^{16}	-1.0	0.0
14	$HO_2 + HO_2 \Leftrightarrow H_2O_2 + O_2$	3.02×10^{12}	0.0	1.39
15	$H_2O_2 + M \Leftrightarrow 2OH + M$	1.20×10^{17}	0.0	45.5
16	$H_2O_2 + H \Leftrightarrow H_2O + OH$	1.00×10^{13}	0.0	3.59
17	$H_2O_2 + H \Leftrightarrow H_2 + HO_2$	4.82×10^{13}	0.0	7.95
18	$H_2O_2 + O \Leftrightarrow OH + HO_2$	9.55×10^{06}	2.0	3.97
19	$H_2O_2 + OH \Leftrightarrow H_2O + HO_2$	7.00×10^{12}	0.0	1.43

Table 2-4: Hydrogen-Air mechanism. Rate constants in the form $k_f = A\,T^{\beta} \exp(-Ea/T)$; units are moles, cm, seconds, K and kcal/mol. Third body coefficients in reactions 5, 6, 7, 8, 9 and 15 enhancement factors are 0.12 for H_2O and 0.25 for H_2.

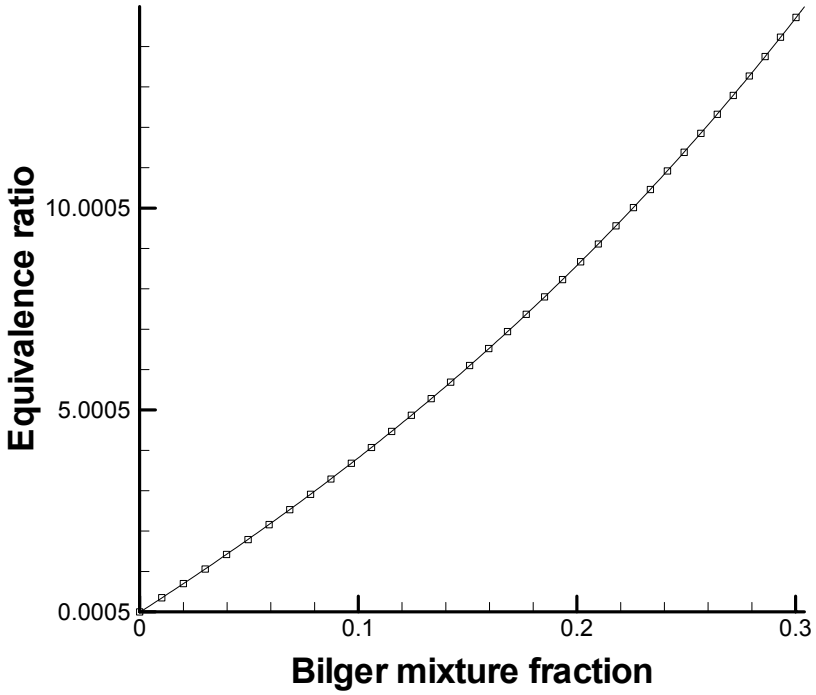

Figure 2-1: Plot of polynomial fit used to obtain the equivalence ratio from the Bilger mixture fraction.

Chapter 3
Results and Discussions

The process of mutual annihilation involves the progressive interactions of the various layers of the flames including the 'preheat' layers and the reaction layers. During each set of interactions, the roles of differential diffusion may be identified for these interactions and subsequent effects on the following layers. These interactions are, also, transient; and therefore, a comparison with steady state behavior is needed. This is achieved by tracking global quantities temporal profiles. Moreover, a reference problem is computed, which corresponds to the case of unity Lewis numbers for all species. Comparison between the non-unity Lewis number and the unity Lewis number computations will help discern the contributions by differential diffusion from those related to finite-rate chemistry. Along with the two stoichiometric flames (at unity and non-unity Lewis numbers), two more cases are considered, which correspond to rich (ø=1.4) and lean (ø=0.7) fuel conditions at non-unity Lewis numbers. This chapter addresses the effect of differential diffusion and finite rate kinetics during the annihilation process for the above three cases.

The mutual annihilation process may be divided into the following stages:

1. Thermo-diffusive interactions: During the first stage, the thermal layer along with reactant's diffusive layers merge at the symmetry plane between the two flames.
2. Reaction layer interactions: During a second stage reactions layers corresponding to the consumption layers of the reactants and the consumption and production layers for the intermediates, and finally the production layers of the products merge.
3. Final burnout: The final burnout may be associated primarily with the depletion of the radical pool, which results in significant decreases in the consumption of remaining intermediate species and reactants.

3.1 Thermo-Diffusive interaction

3.1.1 Evolution of the H_2, O_2 species mass fraction and Temperature profiles along the symmetry line

Figures 3.1 and 3.2 show the evolution of the H_2, O_2 species mass fraction and temperature at the symmetry line for the cases of unity and non-unity Lewis numbers, respectively. The mass fractions are normalized by their initial values and the temperature is normalized to obtain a complimentary progress variable. Before the interactions all three normalized quantities are equal to unity.

For both the cases initially the profiles are flat indicating the absence of any interactions. A change in the profiles indicates the onset of thermo-diffusive interactions. For the unity Lewis number case all the three profiles are similar during the thermo-diffusive interactions. The reason for this similarity is that the reactants and temperature diffuse at the same rates. By imposing unity Lewis numbers, the mass diffusivities of the species are made equal to the thermal diffusivities. However, during the interaction of the reaction layers, the profiles diverge from each other. This is due to the individual contribution of the elementary reactions on the heat generation and reactants consumption.

For the case of non-unity Lewis numbers, the profiles are different even during the thermo-diffusive interactions. This is clearly the effect of differential diffusion as different species and temperature diffuse at different rates. Species H_2 diffuses first from the symmetry line, since it has the lowest Lewis number on the reactants' side, and is followed by the temperature, and finally by the species O_2.

Figures 3.3 and 3.4 show the evolution of normalized H_2, O_2 species mass fraction and temperature for the rich and lean cases, respectively. From the plots, the presence of differential diffusion is evident. An interesting aspect is that H_2 diffuses at a much earlier time from the symmetry line for the lean case as compared to the stoichiometric (non-unity Lewis number) and the rich case. This is due to the difference in the Lewis number of H_2 for the three cases as indicated in Tables 2.1 to 2.3. From Fig. 3.3 for the rich case, we see that the mass fraction of H_2 increases at the symmetry line after the flames have merged. Whereas for the lean case (Fig. 3.4), excess O_2 remains after the flames have merged.

3.1.2 Centerline Evolution of Equivalence ratio

Figures 3.5 to 3.7 show the evolution of the equivalence ratio at the symmetry line for the stoichiometric (non-unity Lewis number), rich and lean cases respectively. For the stoichiometric (non-unity Lewis number) case the equivalence ratio decreases during the thermo-diffusive interactions and by the time the interactions of the reaction layers begin the mixture is lean. This is due to the differential diffusion of H_2 from the centerline into the flame during the thermo-diffusive interactions. For the lean case (see Fig. 3.7), the equivalence ratio, which is less than unity initially further decreases during thermo-diffusive interactions due to the differential diffusion of H_2 away from the centerline. The reacting mixture has an equivalence ratio of approximately 0.4 at the beginning of the reaction layers interactions. For the rich case (see Fig. 3.6), the equivalence decreases during the thermo-diffusive interactions to a composition that is slightly higher than the stoichiometric value.

However, for all the three cases, the equivalence ratio increases during the stage of final burnout. This increase is due to the following reasons;

a) There is diffusion of excess unburnt H_2 from the product side back to the symmetry line increasing the equivalence ratio.
b) Since the equivalence ratio is based on tracking the elements, the presence of the products and intermediates at the centerline leads to an increase in its value.

3.1.3 Evolution of the Leading Edges of the Normalized Temperature and Reactant mass fractions

Figure 3.8 shows the evolution of the leading edges of the normalized temperature, H_2 and O_2 species mass fractions for the stoichiometric (non-unity Lewis number) case. The slopes of the leading edges measure the displacement speeds of the respective iso-contours. The merger of the leading edges is an indicator of the end of thermo-diffusive interactions. From the plot, we see that initially the slopes are constant. As the thermo-diffusive interactions end, the slopes increase, indicating an acceleration of the mutual annihilation process. This acceleration has also been observed in previous studies on methane-air flames by Chen et. al (1995) and Echekki et. al (1996). The sequence of the

merger of the leading edges is consistent with the previous results. The relative time taken by the leading edges is shown in the table below:

Scalar	T	H_2	O_2
Time taken (t/t_f)	0.0390	0.0377	0.0394

Table 3-1: Relative time (normalized by flame time) taken by the leading edges of temperature and reactants to merge with the symmetry line.

3.1.4 Effects of Thermo-Diffusive interactions

During thermo-diffusive interactions except for the unity Lewis number case, the temperature and species diffusive layers merge with the centerline at different times. Thermo-diffusive interaction results in the deficiency of H_2 at the centerline leaving a leaner mixture towards the end of interaction for the stoichiometric (non-unity Lewis number) and lean cases and a stoichiometric mixture for the rich case. This results in a change in the chemical enthalpy of the system. The merger of the temperature layers preheats the mixture. This causes a change in the sensible enthalpy of the system. In the case of unity Lewis numbers, there is no differential diffusion, and hence chemical and sensible enthalpies balance each other.

Since thermo-diffusive interactions bring about a change in the sensible and chemical enthalpies, they have an effect on the final products' temperature and their composition. It also affects the different consumption rates for the reactants and different consumption and production rates for the intermediates.

As the final mixture is lean for the stoichiometric (non-unity Lewis number) case, the flame burns lean. As will be discussed later, the differential diffusion of H_2 results is an increase in the production of species O. These conditions may be favorable for the production of thermal NO.

3.2 Reaction layers interaction

The reaction zone is made of different layers namely the fuel consumption layers where the fuel is oxidized, the radical consumption layers where radicals diffuse towards the reactants to consume the fuel and oxidizer, and the radical production layers where radicals are produced. These layers merge with the centerline at different times. The thermo-diffusive interactions have brought about the depletion of one reactant over the other due to the merger of the diffusive layers and preheat of the reacting mixture due to the merger of the temperature layers.

3.2.1 Evolution of Consumption speed for the reactants

Figures 3.9 to 3.12 show the temporal evolution of the consumption speeds for the reactants H_2 and O_2 for the stoichiometric (unity Lewis number and non-unity Lewis number) case, the rich case and the lean case respectively. The quantities are normalized by their initial values.

First, the stoichiometric (unity Lewis number) case is considered. Figure 3.9 shows the temporal evolution of the consumption speeds of H_2 and O_2 at the symmetry plane between the two annihilating flames. The figure shows that the consumption speeds of both H_2 and O_2 increase prior to rapid decay. The final rapid decay is a result of the merger of the reactions layers that concludes the mutual annihilation process. The initial rise in the consumption speed profiles may be attributed to the balance between the contributions of preheat, which tend to increase the Arrhenius term in the reaction rate, and the role of reactants' depletion at the center, which tends to reduce the concentrations in the expression of the reaction rates. The process of preheat and depletion of reactants occur simultaneously and affect the chemistry. During the initial stages the preheat effect is more dominant than the depletion of the reactants and the consumption speed of the fuel and oxidizer both increase.

Figure 3.10 shows the evolution of the consumption speeds for H_2 and O_2 for stoichiometric (non-unity Lewis number) case. The consumption speed of both H_2 and O_2 start to decrease during the merger of the reaction layers as seen in the initial dip in their values. But the consumption speed of O_2 increases similar to the unity Lewis number

case. Whereas, the consumption speed of H_2 decreases without any initial increase in value prior to decay. The deficiency of H_2 caused by the differential diffusion of H_2 during thermo-diffusive interactions plays a more dominant role on chemistry than preheat caused by the merger of the temperature layers. Hence, the consumption speed of H_2 does not increase.

Figure 3.11 shows the evolution of the consumption speeds of H_2 and O_2 for the rich case. The consumption speeds for both H_2 and O_2 increase prior to rapid decay. For the rich case the mixture is still rich during the beginning of the reaction layer interactions and hence there is no deficiency of H_2 in the mixture. The effects due to the depletion of H_2 by thermo-diffusive interaction are offset by the excess of H_2 present in the mixture. Hence for both the species the reactions responsible for their consumption respond to preheat and increase their rates Thus, increasing their consumption speed.

Figure 3.12 shows the evolution of the consumption speeds of H_2 and O_2 for the lean case. From the figure, we see that the consumption speeds of both the reactants decrease during the course of mutual annihilation without any prior increase in their values. This is because the mixture is lean to start with, thermo-diffusive interactions render the mixture much leaner and this deficiency of H_2 dominates the effect of preheat due to the merger of the temperature layers.

3.2.2 Evolution of reaction rates of progress for the dominant reactions that consume the fuel and the oxidizer

We have seen that the consumption speed for O_2 initially increases at the onset of reaction layer interactions for the stoichiometric (unity and non-unity Lewis number) and the rich cases whereas that of H_2 for stoichiometric (non-unity Lewis number) and lean cases, it does not increase. The next step is to identify the reasons for the variation in the consumption speeds of the reactants prior to mutual annihilation. For this purpose, the evolution of the reaction rates of progress of dominant reactions is considered.

Let us examine the expression for the rate of reaction progress given by Eq. (2.5). The temperature dependency is seen in the rate constant term and the dependency on the reactants is seen in the concentration terms. The merger of the temperature layers brings

about an increase in the temperature of the reaction mixture and the diffusion of the reactants due to thermo-diffusive interactions brings about the deficiency of the reactants. The elementary reactions respond differently to these changes based on their dependencies on temperature and species concentrations.

The first three reactions from table 2.4 are the dominant reactions responsible for the consumption of O_2 and H_2 while merger. They are given by:

	Reaction	**Ea** (kcal/mol)
1	$H + O_2 \Leftrightarrow O + OH$	16.44
2	$O + H_2 \Leftrightarrow H + OH$	6.29
3	$OH + H_2 \Leftrightarrow H_2O + H$	3.43

The activation energy of Reaction 1 is relatively higher than that of Reactions 2 and 3. Figure 3.13 shows the evolution of the reaction rate of progress for the three reactions mentioned above for the stoichiometric (unity Lewis number) case. These are integrated quantities normalized by their initial values. Since there is no deficiency of one reactant over the other due to differential diffusion all the three reactions respond to the preheat due to the merger of the temperature layers by increasing their reaction rates. This is indicated in the plot where the integrated reaction rates of progress for the three reactions increase based on their relative magnitude of activation energy just before they decay rapidly. The rapid decay is due to the merger of their respective layers with the symmetry plane.

Figure 3.14 shows the evolution of the integrated reaction rates of progress for the same three reactions for the stoichiometric (non-unity Lewis number) case. In this case there is deficiency of H_2 due to the thermo diffusive interactions. Reaction 1 has higher activation energy, and there is no deficiency of O_2. Therefore, it responds to preheat by increasing its reaction rate. The deficiency of the fuel (H_2) due to differential diffusion offsets this effect of preheat in the case of Reaction 2 and to a greater extent in Reaction 3. The integrated reaction rate of progress for Reaction 2 does not increase to the same extent as in the unity Lewis number case and that of Reaction 3 just decreases. It is interesting to note that the reaction layer of 3 is the first to merge with the centerline followed by that of Reactions 2 and 1.

Figure 3.15 shows the evolution of the integrated reaction rates of progress for the same three reactions for the rich case. In this case the deficiency of H_2 caused by differential diffusion during thermo-diffusive interactions is compensated by the presence of excess H_2 in the reacting mixture (rich condition). During the merger of the reaction layers the mixture is stoichiometric as indicated by Fig. 3.6. This condition, coupled with the effect of preheat increases the reaction rate of all the three reactions.

Figure 3.16 shows the evolution of the integrated reaction rates of progress for the same three reactions for the lean case. Differential diffusion of H_2 during thermo-diffusive interactions further intensifies the deficiency of H_2. This deficiency plays a more dominant role over the effect of preheat and none of the reactions increase their reaction rates.

The increase in the reaction rate of the first two reactions brings about the increase in the consumption of fuel and oxidizer but also results in an increase production of the species OH. This is true for all the cases except the lean case. The consequences of which will be discussed during the interaction of the radical layers.

3.2.3 Evolution of consumption and production layers of radicals

The radical reaction layers consist of both consumption and production layers. Some of the radicals have more than one such layer. The consumption layer closer to the reactant side is the first to merge. It merges with the merger of fuel consumption layers. This merger is followed by the merger of the production layer. Finally the annihilation is complete with the merger of the second consumption layer at the symmetry line. The second consumption layer corresponds to the burnout region where radical recombination reactions consume the radicals. The merger of the first consumption layer initially increases the mass fraction of the radicals followed by rapid decay due to the merger of the production layers. The trend continues into the burnout stage where the radical pool is further depleted.

For the purpose of illustration the species O is considered. Figure 3.17 shows the evolution of the integrated consumption and production layers of the species O for the stoichiometric (unity Lewis number) case. These quantities are normalized by their initial

values. The consumption layer I is the first to merge followed by the merger of the production layer I, which increases in magnitude prior to rapid decay. And finally the consumption layer II merges with the symmetry line indicating the burnout stage. The increase in the magnitude of the production layer I is due to an increase in the reaction rates of certain reactions responsible for the production of the species O, which will be discussed in the following section. The oscillatory nature is due to the process of integration where at different times parts of the consumption layer are omitted or parts of the production layers are added.

Figure 3.18 shows the evolution of the integrated consumption and production layers of the species O for the stoichiometric (non-unity Lewis number) case. The consumption layer I merges first, followed by the merger of the production layer I. The increase in the magnitude of production layer I is much more pronounced for this case as compared to the unity Lewis number case. This increase in the production mechanism increases the mass fraction of species O until the merger of the consumption layer II.

Figure 3.19 shows the evolution of the integrated consumption and production layers of species O for the rich case. The results are normalized by their initial values. The increase in the production rate for this case is greater than compared to the stoichiometric (non-unity Lewis number) case.

Figure 3.20 shows the evolution of the integrated consumption and production layers of species O for the lean case. The sequence of merger is the similar to the previous cases. In this case, the production layer reduces in magnitude much earlier to annihilation and during merger it increases slightly and decays rapidly after that.

3.2.4 Evolution of the intermediate species mass fraction

The intermediate species mass fractions increase initially before their rapid decay caused by the process of annihilation. This increase is due to the merger of the first consumption layers and may be coupled with the increase in magnitude of the production layers prior to their decay. The merger of the consumption layer leaves behind the radicals without being consumed and initially there is an increase in their mass fractions. For the species O the increase in its mass fraction is due to both merger of the consumption layer I and an increase in the magnitude of the production layer. Figure 3.21 shows the evolution of the

mass fraction of O for the stoichiometric (unity Lewis number) case. Figures 3.22 and 3.23 show the evolution of the mass fraction of O for stoichiometric (non-unity Lewis number) and rich case respectively. The increase in the mass fraction of O for the above cases is based on an initial increase in the magnitude of the production reactions. After the production layers have merged the mass fraction of O decreases, and the trend continues with the merger of the second consumption layer.

3.2.5 Evolution of the reactions responsible for the increase in production layer of species O

In the previous sections, we have observed an increase in the production rates of species O for the stoichiometric (unity and non-unity Lewis number) and the rich cases, resulting in an increase in its mass fraction. In this section the mechanisms responsible for this increase in production rates are discussed. As mentioned earlier. Reactions 1 and 2 respond to preheat by increasing their reaction rates, resulting in an increased rates production of species OH. Also Reaction 3, which consumes OH, is the first to merge with the symmetry line along with the fuel consumption layer. As a result, there is an increase in the concentration of OH towards the end of annihilation of the flames.

Reaction 4: $OH+OH \Leftrightarrow O+H_2O$ is a radical recombination reaction producing O and the product H_2O. This reaction along with the reaction 1 is responsible for the production of O. The merger of reaction layer of 1 leaves reaction 4 as the chief producer of O. Due to an increase in the concentration of OH; reaction 4 increases its rate resulting in an increase in the production of O.

Figure 3.24 shows the evolution of the reaction rate of progress of reactions 3 and 4 for the stoichiometric (unity Lewis number) case. In this case there is no deficiency of H_2 during thermo-diffusive interaction due to the absence of differential diffusion. Hence reaction 3 increases its rate before merging as seen in the plot. Also the rate of reaction 4 does not increase and the only way the production layer I can increase is due to an increase in the reaction rate of 1 as seen in Fig. 3.13.

Figures 3.25 and 3.26 show the evolution of the reaction rate of progress of 3 and 4 for the stochiometric (non-unity Lewis number) and the rich cases. Due to the deficiency of H_2 rate of reaction 3 reduces for the stoichiometric (non-unity Lewis number) case. Thus,

momentarily there is an increase in the concentration of OH. Reaction 4 responds to this by increasing its reaction rate. For the rich case the effects of differential diffusion of H_2 are complimented by the rich condition and reaction 3 increases its rate. Since reaction layer 3 still merges ahead of 4 there is an increase in the concentration of OH for which reaction 4 responds by increasing its reaction rate. Thus, there is an increase in the production mechanism of O.

3.3 Burnout stage

The burnout stage is characterized by the depletion of the radical pool due to the radical recombination reactions. From the plots of equivalence ratio and the centerline evolution of H_2 mass fraction it is seen that there is an increase in the amount of H_2 at the centerline during the burnout stage. The reasons for the increase in the equivalence ratio can be illustrated by looking at the evolution of the species mass fraction of H_2 and the spatial distribution of the right-hand side terms of the species equation for H_2 at two different times; one before thermo-diffusive interaction and the other during the burnout stage. These are illustrated for the stoichiometric (non-unity Lewis number) case.

3.3.1 Evolution of the species mass fraction of H_2 for non-unity Lewis number

Figure 3.27 shows the evolution of the species mass fraction of H_2. As seen in the previous sections H_2 diffuses earlier from the centerline during the thermo-diffusive interactions. It diffuses further into the product side as unburnt reactant. Towards the end of the reaction layers interaction the unburnt H_2 diffuses back into the centerline.
To illustrate the diffusion of H_2 into the product side before interactions and back to the centerline during the burnout stage the plot of the right-hand side of the species equation for H_2 is considered. Figures 3.28 and 3.29 show the spatial evolution of the unsteady term, convective term, diffusion term and the reaction term at two different times one before thermo-diffusive interactions and another after reaction layers interaction. The negative sign for the convective and diffusive terms indicates the removal of the species from that location and the positive sign indicates transfer of the species to that location.

The negative sign in the reaction term indicates the consumption of the species from that location and the positive sign indicates the production of the species at that location. Figure 3.28 shows that H_2 diffuses from the centerline into the reaction zone where it is consumed, and diffuses further into the product side as unburnt reactant. Figure 3.29 shows that H_2 diffuses from the product side back to the centerline. Therefore, the equivalence ratio increases during the burnout stage of the interactions.

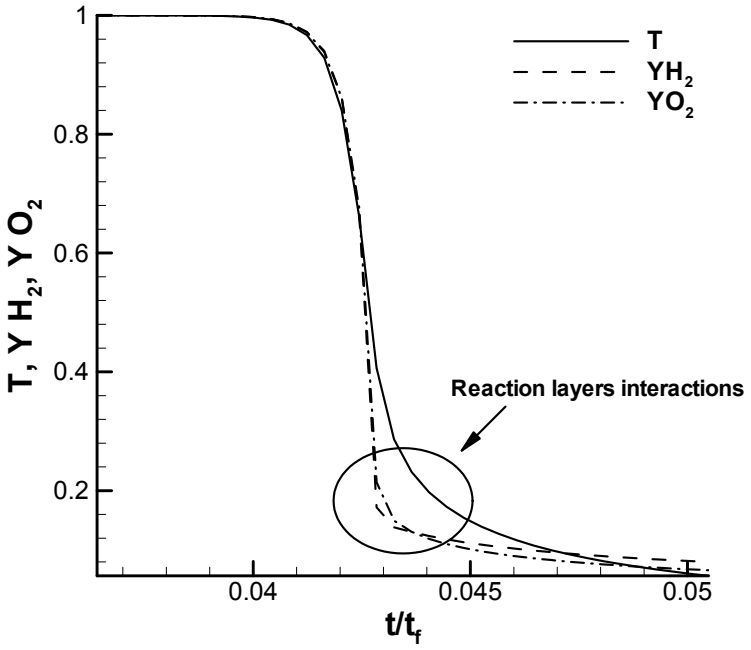

Figure 3-1: Evolutions of the normalized H_2, O_2 species mass fractions and temperature along the symmetry line for the stoichiometric (unity Lewis number) case.

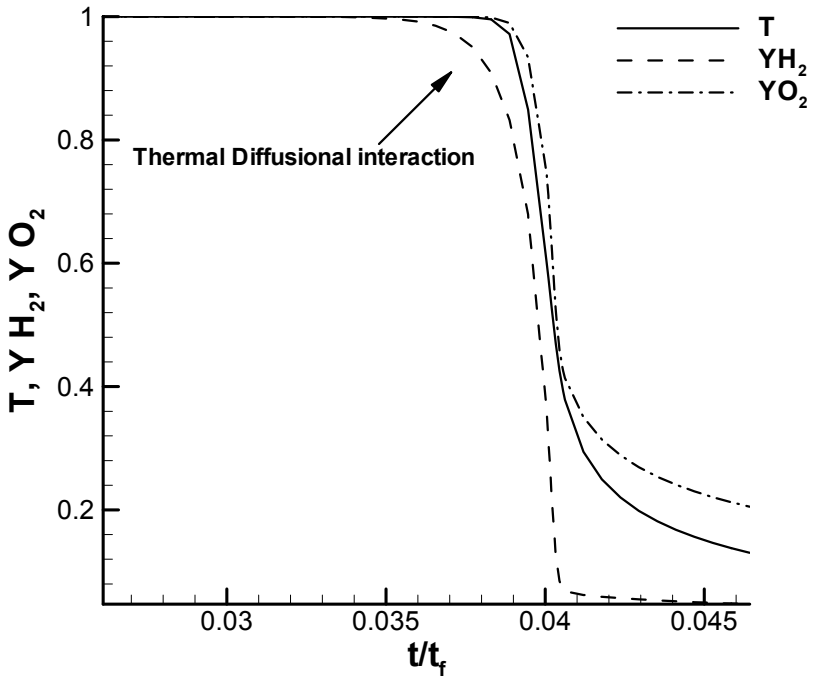

Figure 3-2: Evolutions of the normalized H_2, O_2 mass fractions and Temperature along the symmetry line for the stoichiometric (non-unity Lewis number) case.

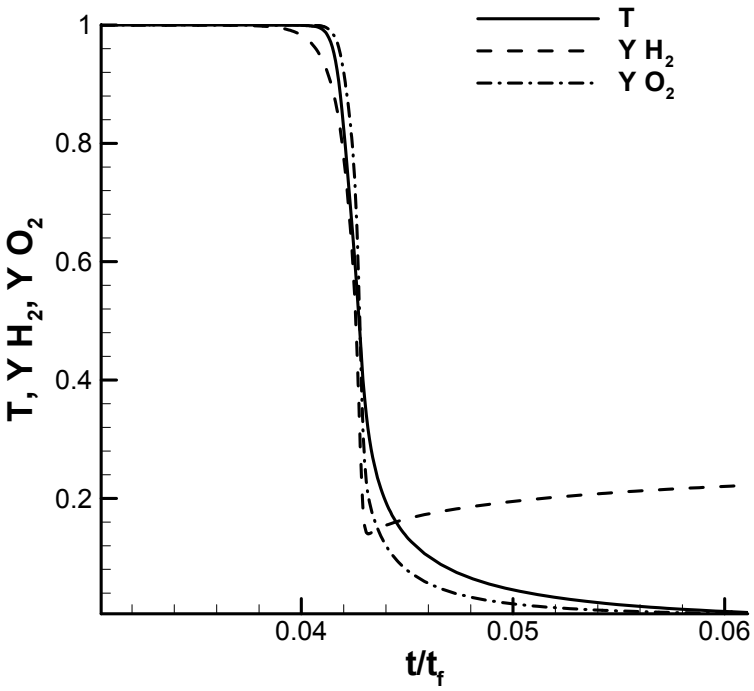

Figure 3-3: Evolutions of the normalized H_2, O_2 mass fractions and Temperature along the symmetry line for the rich case.

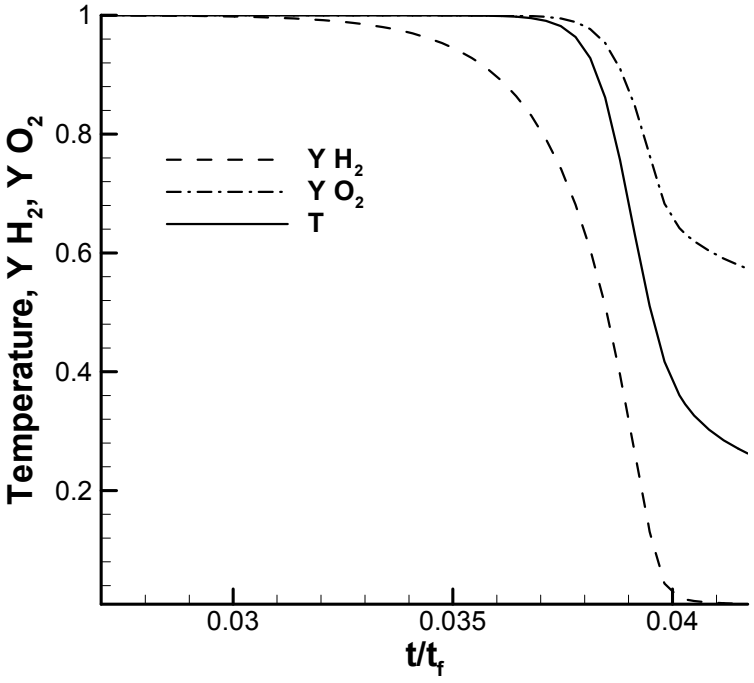

Figure 3-4: Evolutions of the normalized H_2, O_2 mass fractions and Temperature along the symmetry line for the lean case.

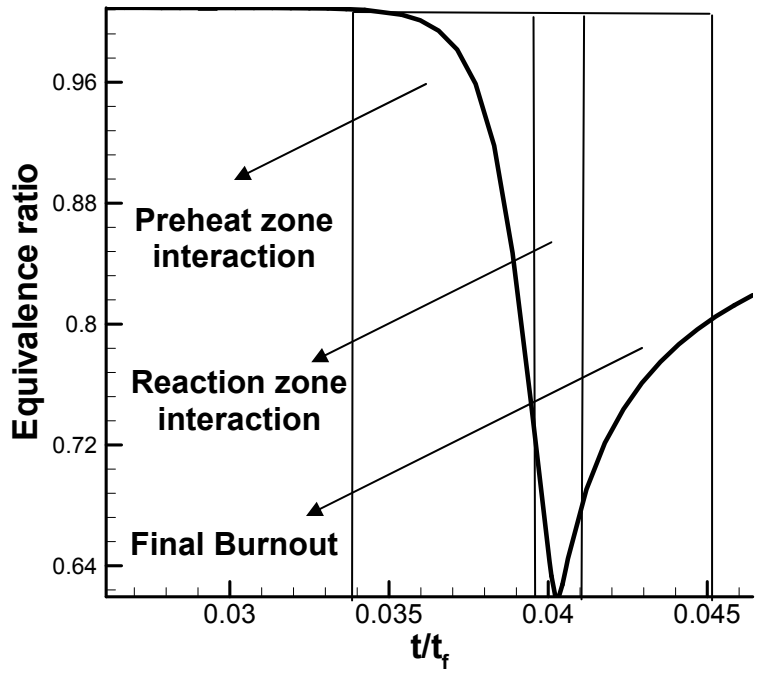

Figure 3-5: Evolution of the equivalence ratio at the symmetry line for the stoichiometric (non-unity Lewis number) case.

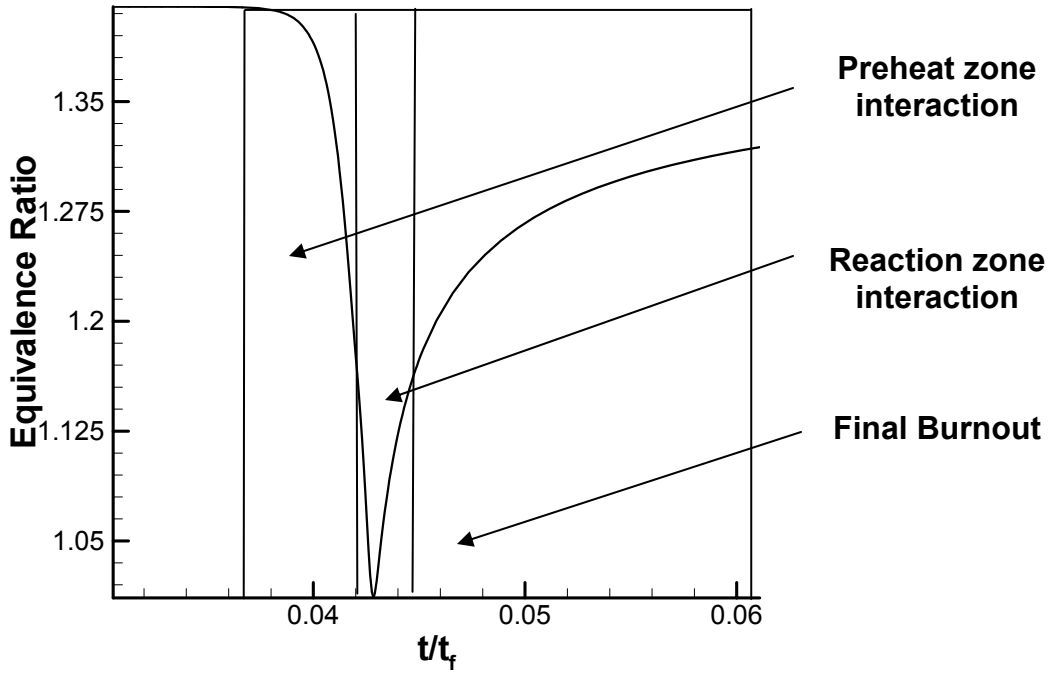

Figure 3-6: Evolution of the equivalence ratio at the symmetry line for the rich case.

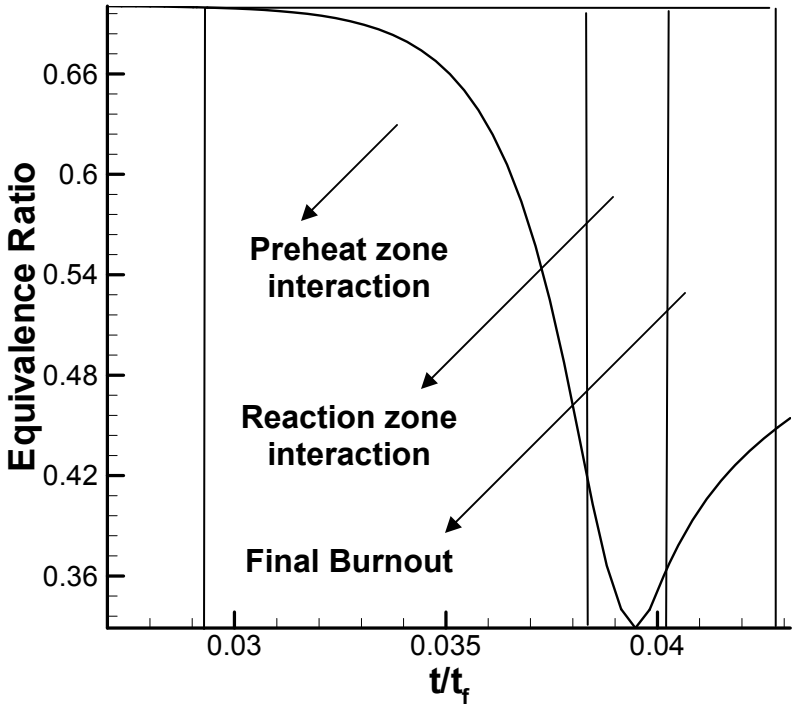

Figure 3-7: Evolution of the equivalence ratio at the symmetry line for the lean case.

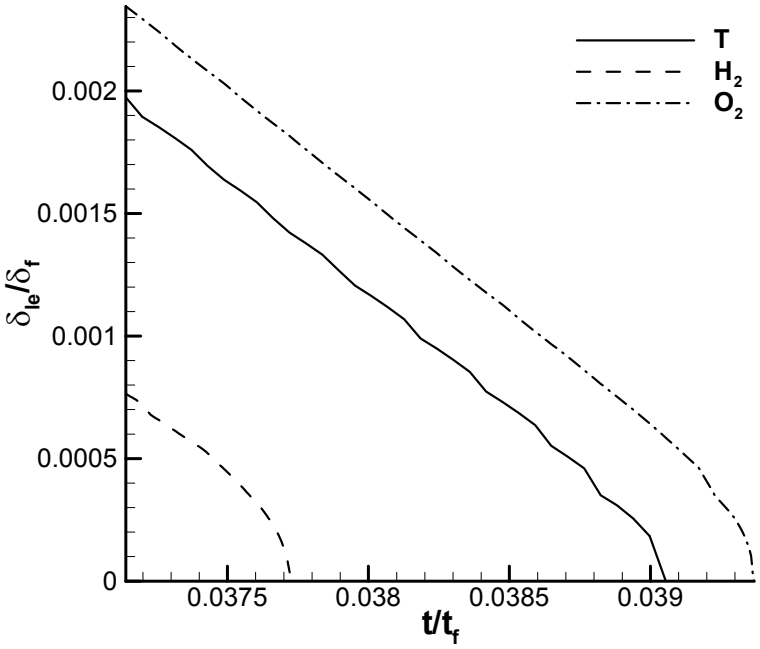

Figure 3-8: Evolution of the Leading edges of the normalized Temperature and reactant mass fractions for the stoichiometric (non-unity Lewis number) case.

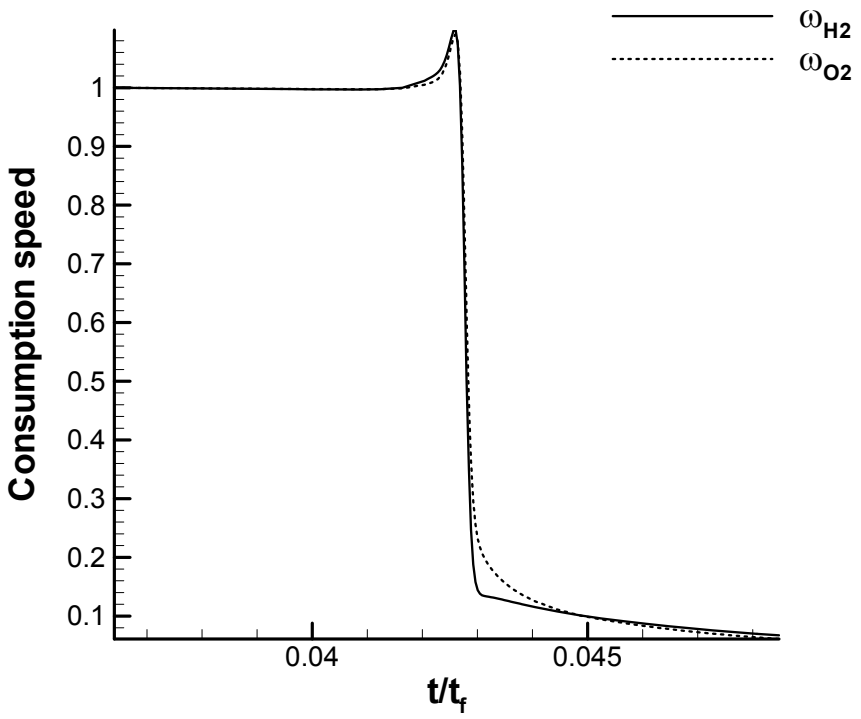

Figure 3-9: Evolution of the normalized consumption speeds of the reactants for the stoichiometric (unity Lewis number) case.

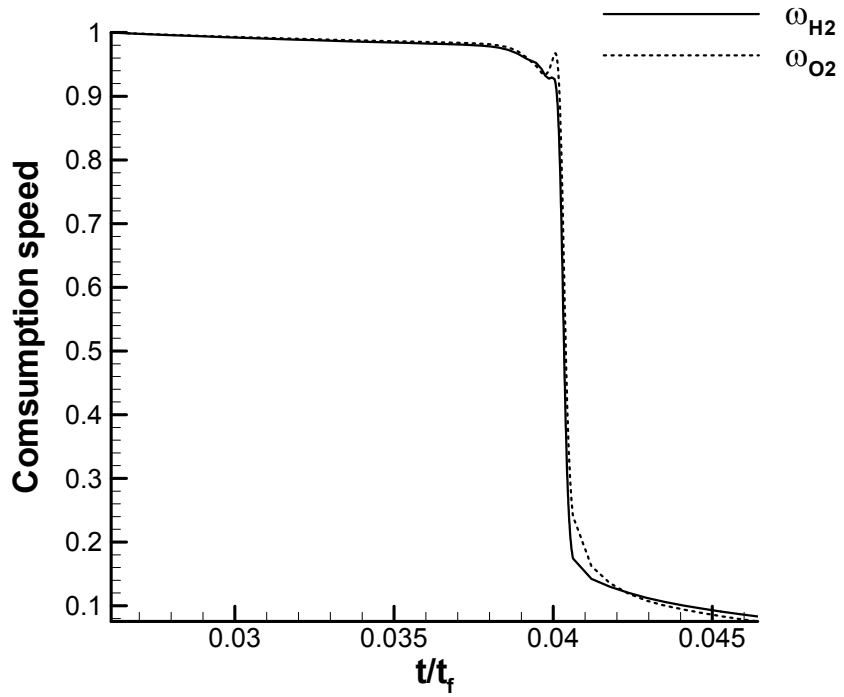

Figure 3-10: Evolution of the normalized consumption speeds of the reactants for the stoichiometric (non-unity Lewis number) case.

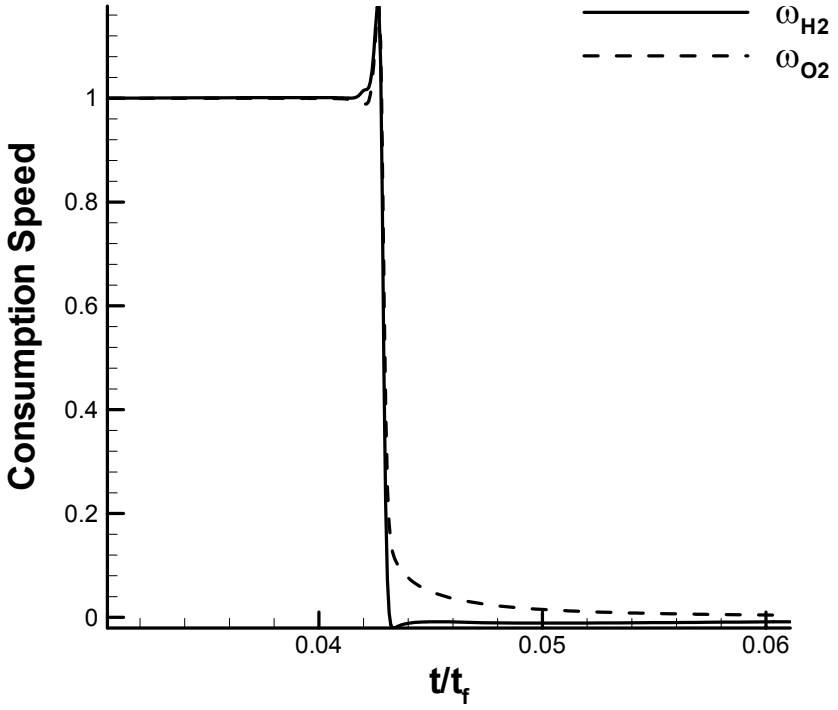

Figure 3-11: Evolution of the normalized consumption speeds of the reactants for the rich case.

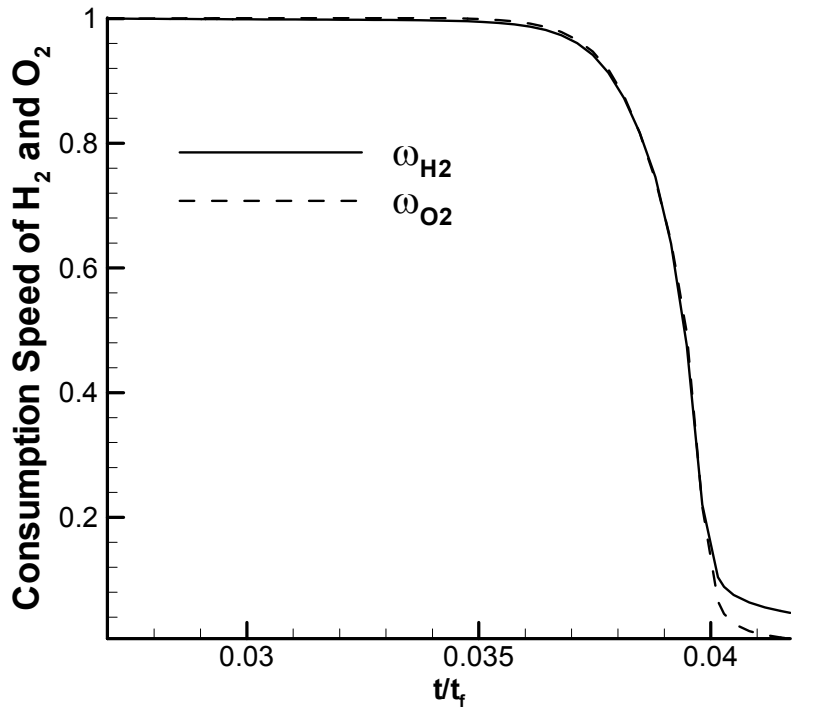

Figure 3-12: Evolution of the normalized consumption speeds of the reactants for the lean case.

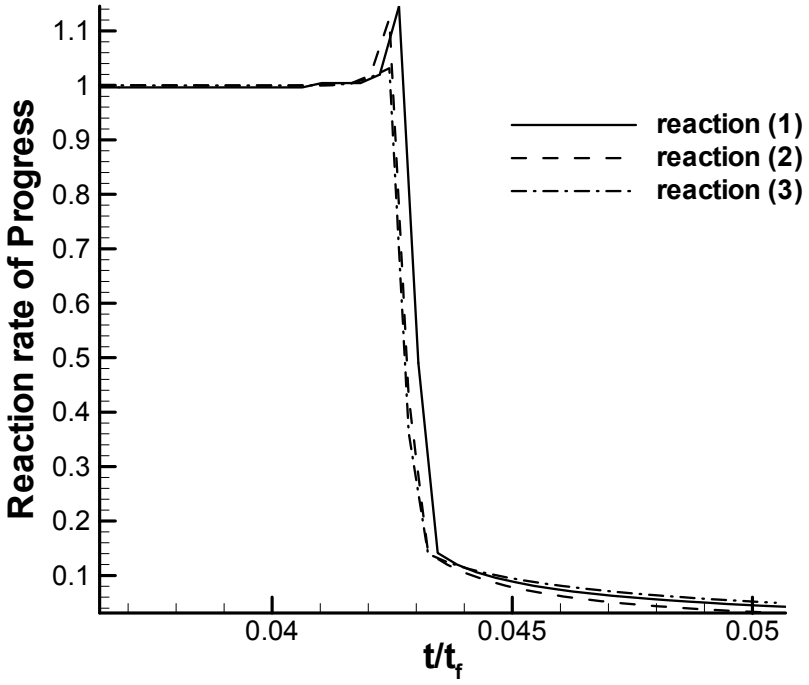

Figure 3-13: Evolution of normalized reaction rate of progress for the dominant reactions consuming fuel and oxidizer for the stoichiometric (unity Lewis number) case.

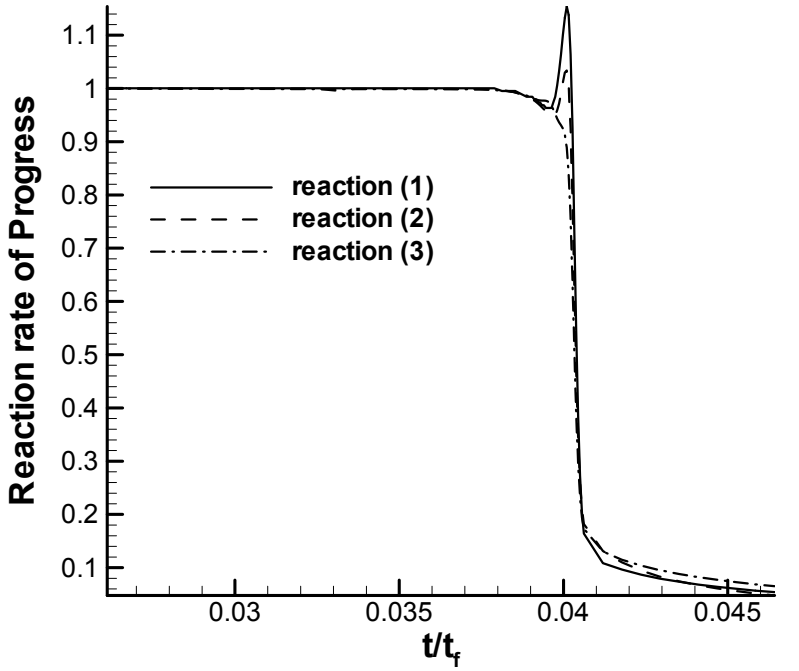

Figure 3-14: Evolution of normalized reaction rate of progress for the dominant reactions consuming fuel and oxidizer for the stoichiometric (non-unity Lewis number) case.

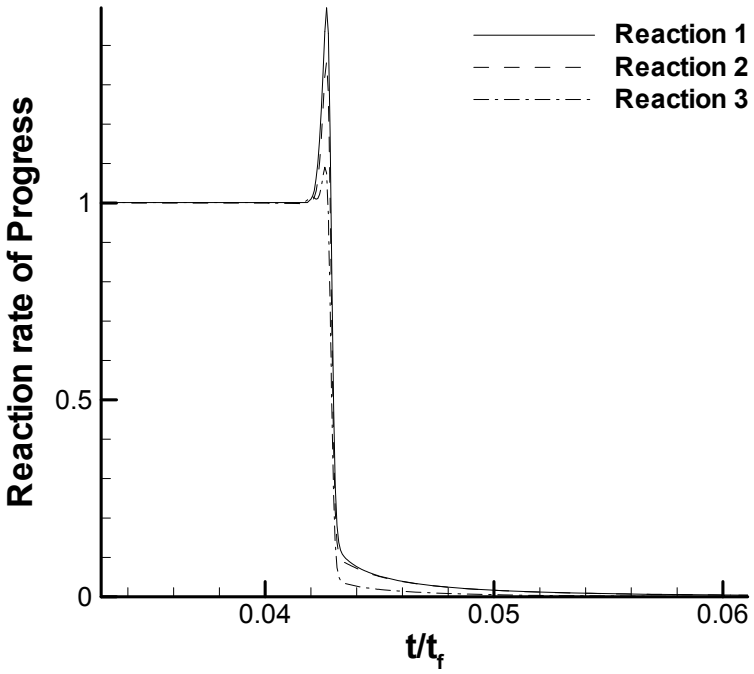

Figure 3-15: Evolution of normalized reaction rate of progress for the dominant reactions consuming fuel and oxidizer for the rich case.

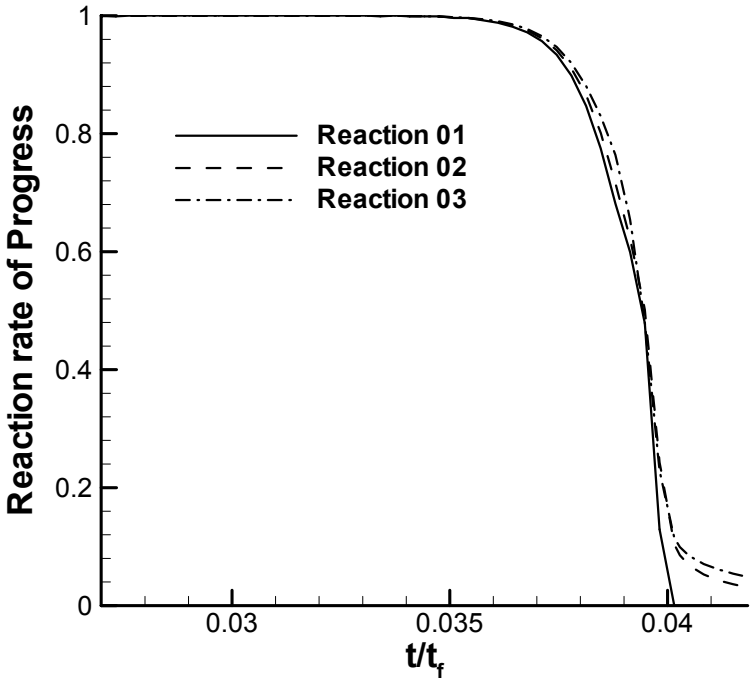

Figure 3-16: Evolution of normalized reaction rate of progress for the dominant reactions consuming fuel and oxidizer for the lean case.

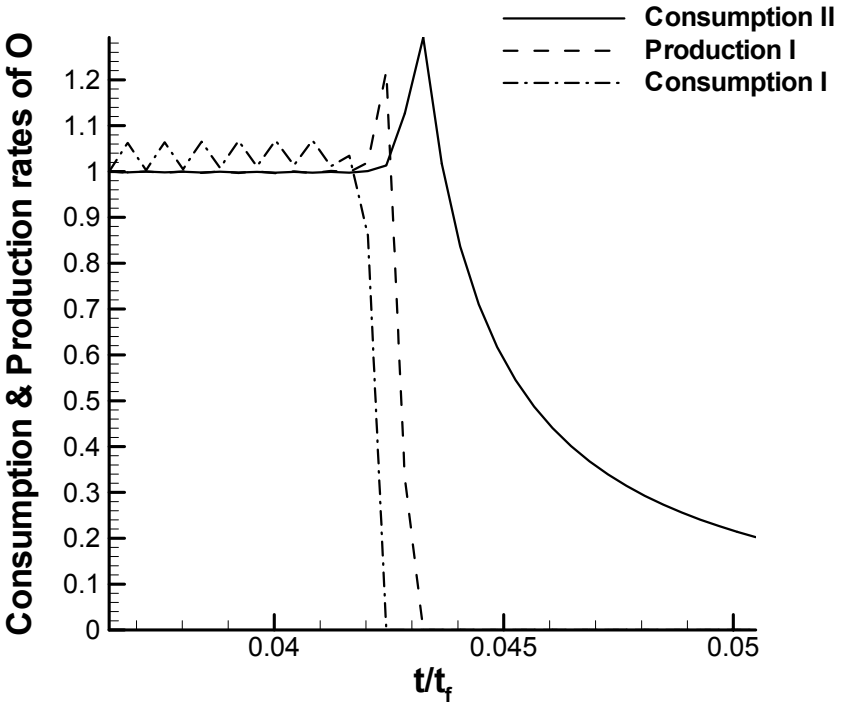

Figure 3-17: Evolution of the normalized reaction layers of species O for the stoichiometric (unity Lewis number) case.

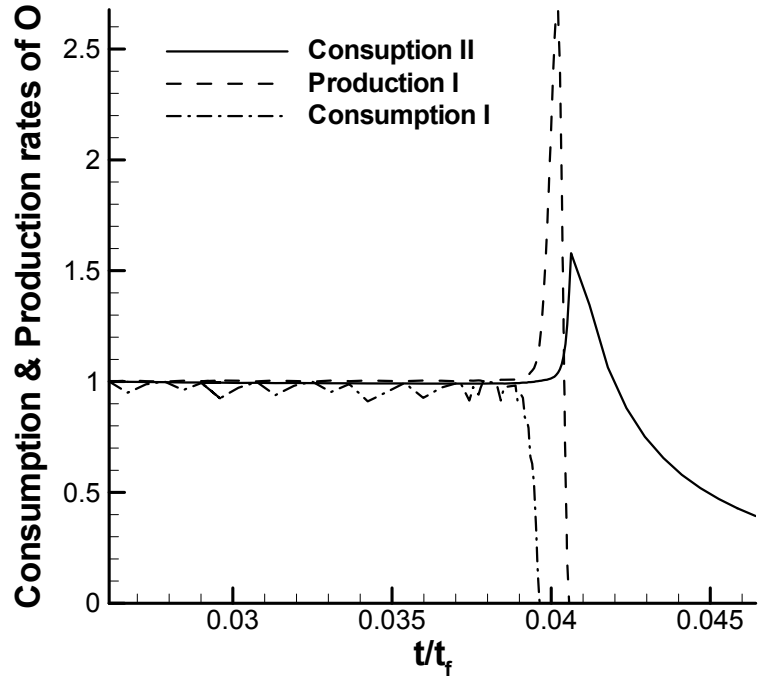

Figure 3-18: Evolution of the normalized reaction layers of species O for the stoichiometric (non-unity Lewis number) case.

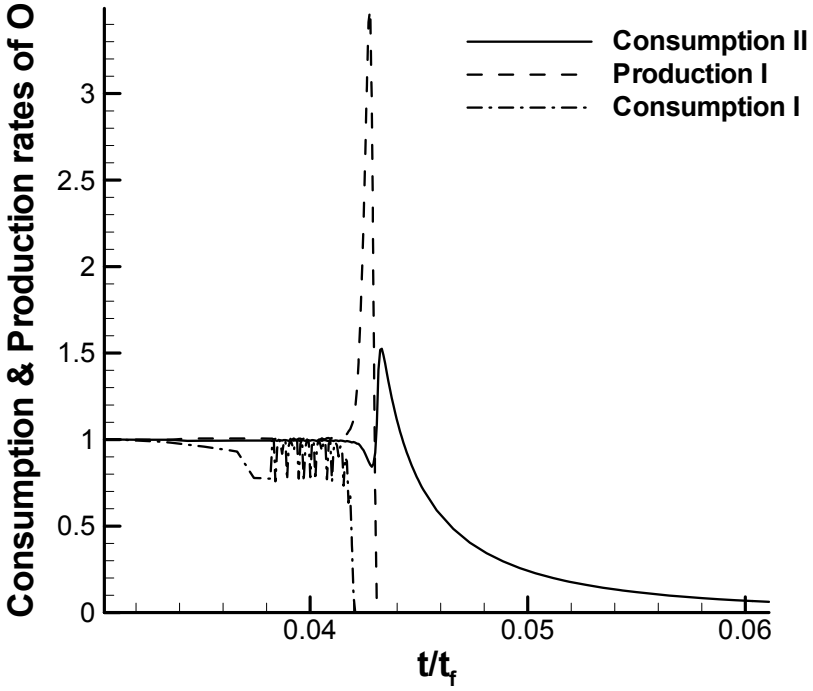

Figure 3-19: Evolution of the normalized reaction layers of species O for the rich case.

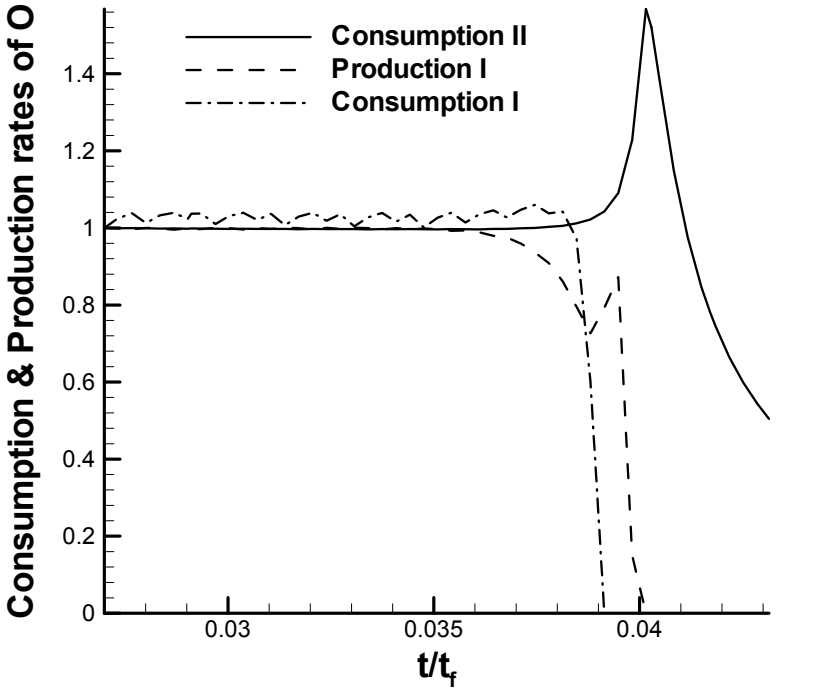

Figure 3-20: Evolution of the normalized reaction layers of species O for the lean case.

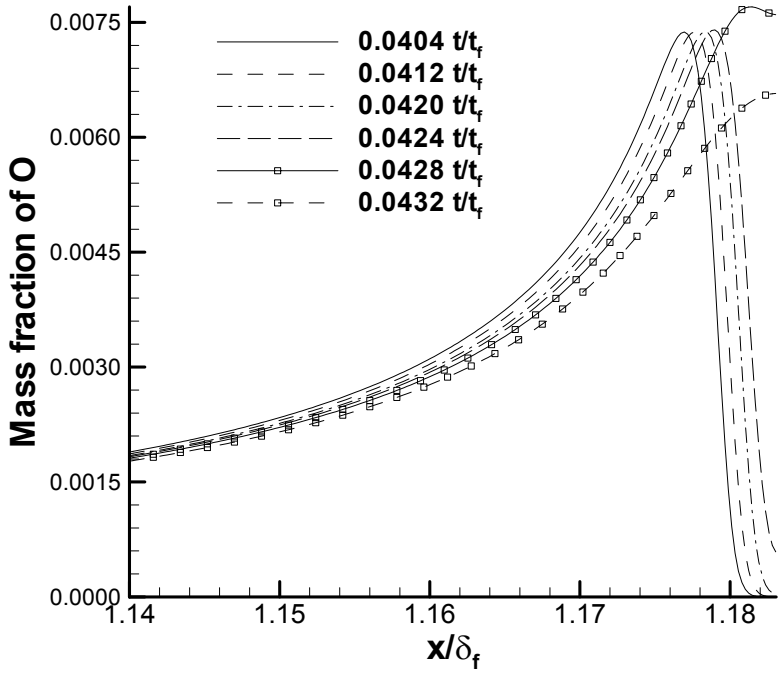

Figure 3-21: Evolution of the species mass fraction of O for the stoichiometric (unity Lewis number) case.

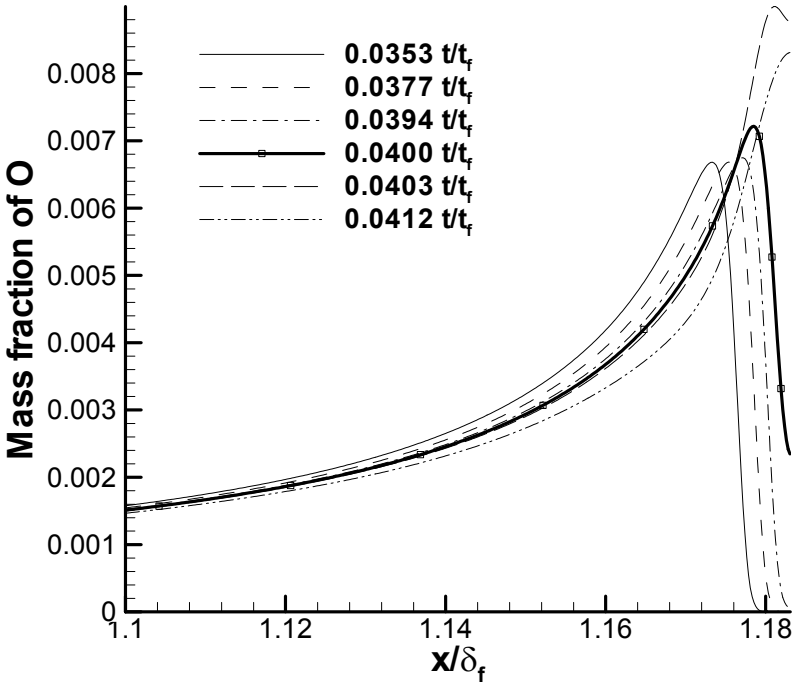

Figure 3-22: Evolution of the species mass fraction of O for the stoichiometric (non-unity Lewis number) case.

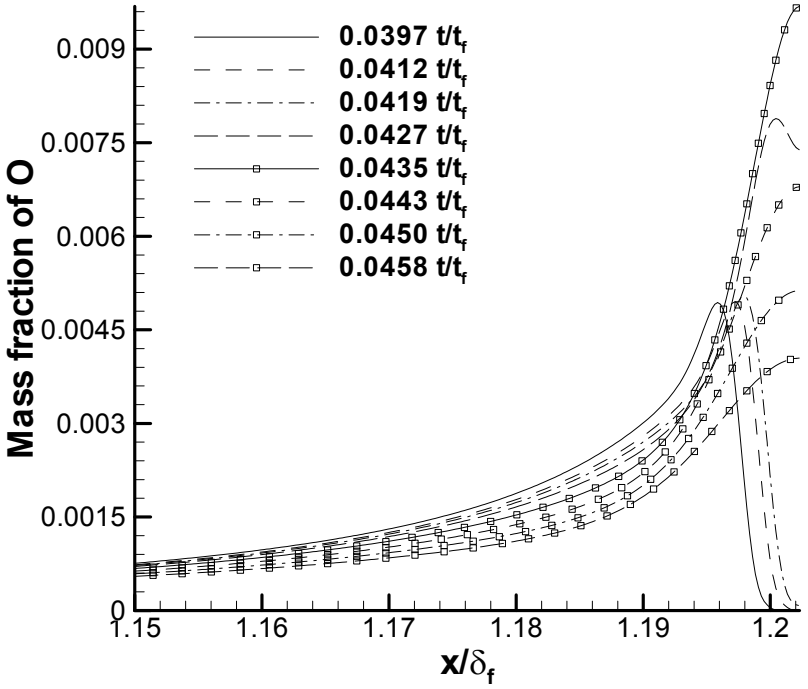

Figure 3-23: Evolution of the species mass fraction of O for the rich case.

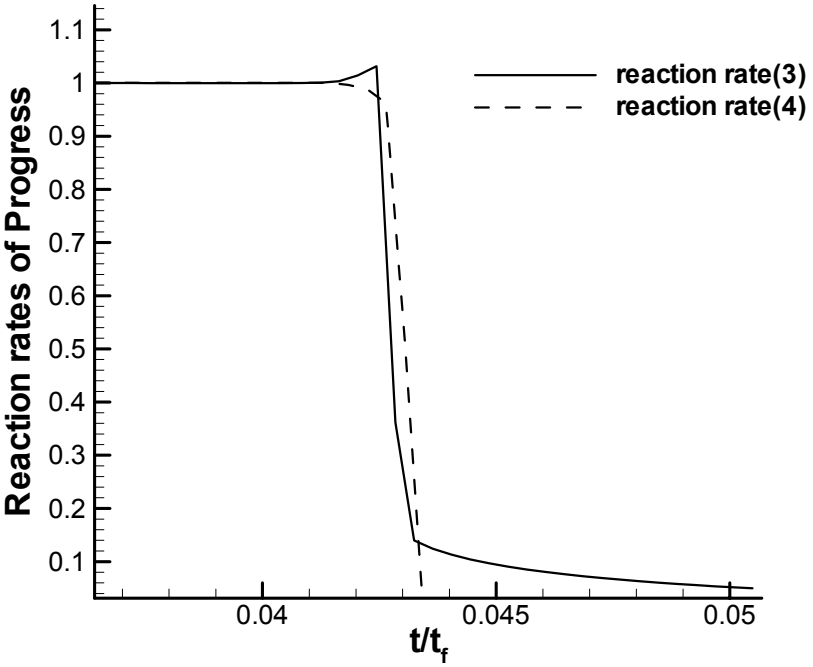

Figure 3-24: Evolution of the reaction rates of progress of reaction 3 and 4 for stoichiometric (unity Lewis number) case.

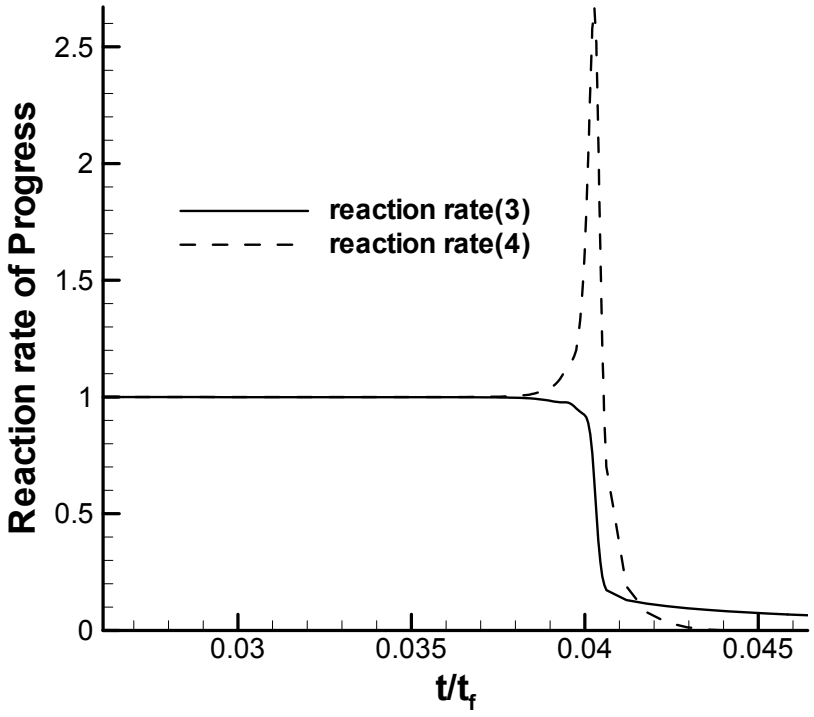

Figure 3-25: Evolution of the reaction rates of progress of reaction 3 and 4 for stoichiometric (non-unity Lewis number) case.

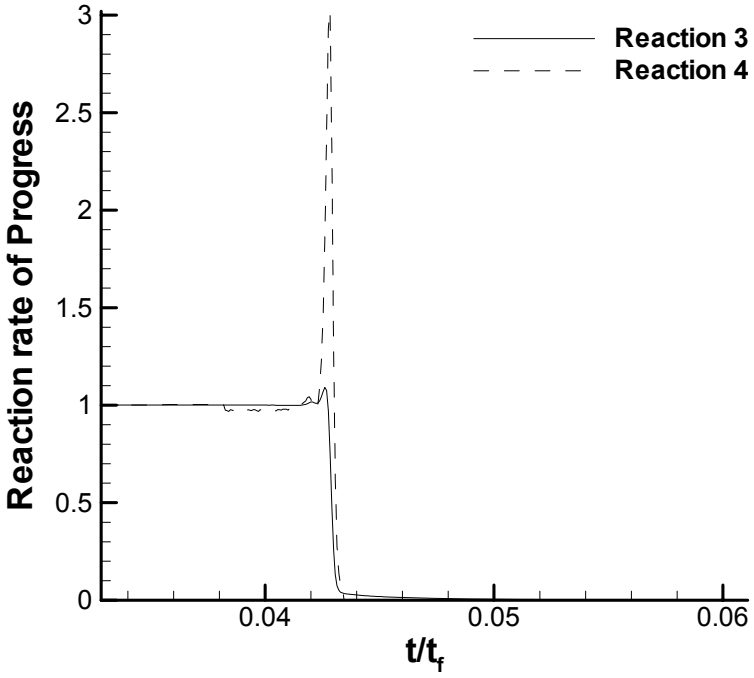

Figure 3-26: Evolution of the reaction rates of progress of reaction 3 and 4 for the rich case.

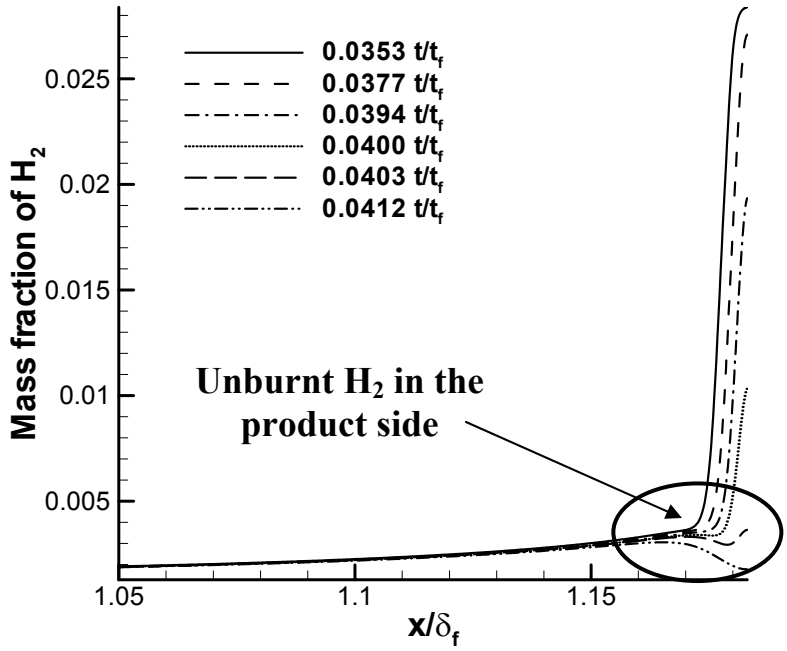

Figure 3-27: Evolution of the species mass fraction of H_2 for the stoichiometric (non-unity Lewis number) case.

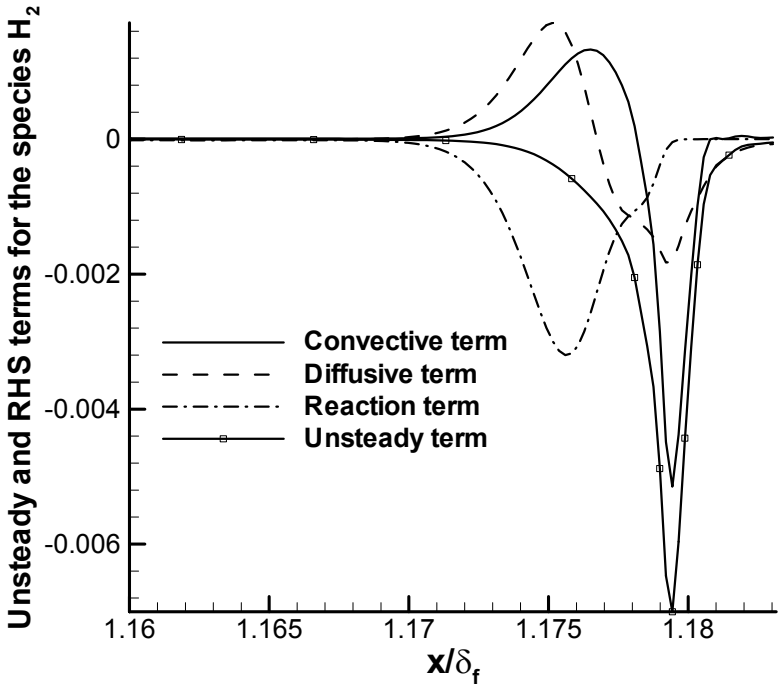

Figure 3-28: Plot of the right-hand side and unsteady terms from the species equation for H_2 at an earlier time before thermo-diffusive interactions for stoichiometric (non-unity Lewis number) case.

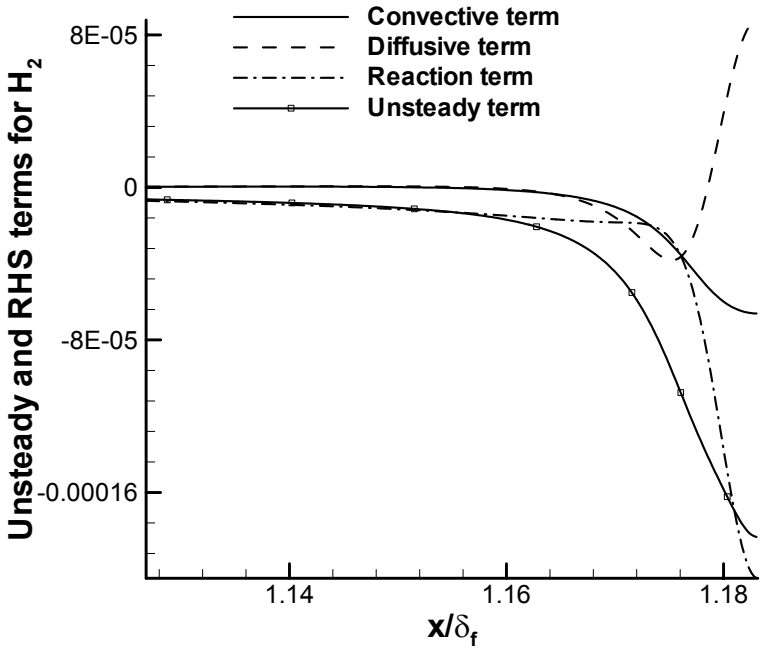

Figure 3-29: Plot of the right-hand side and unsteady terms from the species equation for H_2 at a later time during the burnout stage for stoichiometric (non-unity Lewis number) case.

Chapter 4
Conclusions

In this chapter a synthesis of the computational results is presented. The process of Mutual annihilation of two Hydrogen-Air flames at three equivalence ratios, stoichiometric, rich and lean is studied. It is found that differential diffusion of H_2 plays an important role during the initial stages of interaction and hence determines the final product's composition and temperature.

The interactions take place in different stages namely

- Thermo-diffusive interactions :
    - During this differential diffusion of H_2 causes a leaner mixture at the symmetry line and the flame burns lean for the stoichiometric (non-unity Lewis number) case. There is a shift in the total enthalpy due to the differential diffusion of species and heat.
    - For the rich case there is excess H_2 present in the reaction mixture. This offsets the effect of differential diffusion and the flame is stoichiometric after thermo-diffusive interaction.
    - For the leaner condition there is a deficiency of H_2 in the initial mixture. The thermo-diffusive interaction further brings about the depletion of H_2 from the reaction mixture.
- Interactions of the reaction layers :
    - The deficiency of one reactant over another caused during thermo-diffusive interactions for the stoichiometric (non-unity Lewis number) case leads to different consumption speeds for the fuel and oxidizer during the merger of their respective consumption layers.
    - For the stoichiometric (non-unity Lewis number) case the differential diffusion of H_2 causes an earlier merger of reaction layers consuming OH and the fuel there by aiding the radical recombination reactions leading to an increase in the production of O.

- For the rich case there is abundance of H_2 in the reaction mixture; this offsets the effect of differential diffusion on the rates for reactions consuming the fuel and results is an increase in the radical pool. The merger of OH and fuel consumption layer momentarily increases the concentration of OH. This results in an increase in the rates of radical recombination reactions leading to an increase production of species O.
- For the lean case the deficiency of H_2 initially present and further intensified by differential diffusion offsets the effect of preheat on the reactions consuming the fuel. Thus, there is no increase in the consumption speeds of the reactants prior to annihilation.
- For the stoichiometric (non-unity Lewis number) case the flame towards the end of the reaction layers interaction burns lean and has a higher concentration of the specie O in it. This condition is suitable for the production of thermal NO_x.

- Final Burnout:

  This stage follows the merger of the fuel consumption and radical production layers. Final burnout is associated with the depletion of the radical pool which subsequently results in the quenching of the flame. Also there is diffusion of H_2 back into the centerline from the product side during this stage there by increasing the equivalence ratio.

References

1. Bilger, R.W., Starner, S. H., Kee, R. J., Combust. Flame 80 (1990) 135-149.
2. Candel, S. M., Veynante, D., Lacas, F., Maistret, E., Darabiha, N., and Poinsot, T., in *Recent advances in Combustion Modelling*, in Series on Advances in Mathematics for Applied Sciences (B. E. Larrouturou, ed.), World Scientific, Singapore, 1990.
3. Chen, C.L., and Sohrab, S.H., Combust. Flame 101:360-370 (1995).
4. Echekki, T., Chen, J.H., and Gran, I., The mechanism of mutual annihilation of stoichiometric premixed methane-air flames, in *Proceedings of 26th Symposium (International) on Combustion*, pages 855-863, Pittsburgh, 1996. The Combustion Institute.
5. Im, H.G. and Chen, J.H., Preferential diffusion effects on the burning rate of interacting turbulent premixed hydrogen-air flames, Combust. Flame, 131:246-258(2002).
6. Kee, R.J., Rupley, F.M., Miller, J. A., Sandia National Laboratories report SAND-8215B, 1987.
7. Kennedy, C.K., Carpenter, M.H., Applied Numerical Mathematics, 14 (1994) 397-433.
8. Kennedy, C. K., Carpenter, M. H., Lewis, R. M., Applied Numerical Mathematics 35 (2000) 177-219.
9. Mahalingam, S., Private Communications, 1993.
10. Poinsot, T., Lele, S. J., Comput. Phys. 101 (1991) 1.
11. Smooke, M. D., Giovangigli, V., Reduced kinetic mechanisms and asymptotic approximation for methane-air flame. In: Lecture Notes in Physics 384, (Smooke, M.D., editor). Springer-Verlag, New York, 1991. pp. 1-28.
12. Wichman, I. S., and Vance, R., A study of one-dimensional laminar premixed flame annihilation, Combust. Flame, 110:508-523, 1997.
13. Yetter, R. A., Dryer, F. L., Rabitz, H., Combust. Sci. Tech. 79 (1991) 97-128